ACS OMEGA

http://pubs.acs.org/journal/acsodf

Article

Bioprinting of a Blue Light-Cross-Linked Biodegradable Hydrogel Encapsulating Amniotic Mesenchymal Stem Cells for Intrauterine Adhesion Prevention

Miao Feng,[#] Shengxue Hu,[#] Weibing Qin, Yunge Tang, Rui Guo,[*] and Liwei Han[*]

Cite This: *ACS Omega* 2021, 6, 23067−23075

Read Online

ACCESS | Metrics & More | Article Recommendations

ABSTRACT: Intrauterine adhesion (IUA) is a common and prevailing complication after uterine surgery, which can lead to clinical symptoms such as a low menstrual volume, amenorrhea, periodic lower abdominal pain, infertility, and so on. Placing a three-dimensional printing hydrogel between the injured site and the adjacent tissue is considered to be a physical barrier to prevent adhesion, which can isolate the damaged area during the healing process. In this work, a tissue hydrogel with various proportions of a methacrylated gelatin (GelMA) and methacrylated collagen (ColMA) composite hydrogel loaded with amniotic mesenchymal stem cells (AMSCs) was constructed by using three-dimensional biological printing technology. Compared with the single GelMA hydrogel, the composite antiadhesion hydrogel (GelMA/ColMA) showed an appropriate swelling ratio, enhanced mechanical properties, and impressive stability. Meanwhile, the microstructure of the GelMA/ColMA composite hydrogel showed a denser and interconnected microporous structure. In addition, the cytotoxicity study indicated that the GelMA/ColMA hydrogel has a cytocompatibility nature toward AMSCs. Finally, the fabrication of stem cell encapsulation hydrogels was studied, and the cells could be released continuously for more than 7 days with the normal cell function. The results of in vivo experiments indicated that the GelMA/ColMA/hAMSC (human amnion mesenchymal stem cell) hydrogel can prevent cavity adhesion in a rat IUA model. Therefore, bioprinting a biodegradable hydrogel cross-linked by blue light has satisfactory anticavity adhesion effects with excellent physical properties and biocompatibility, which could be used as a preventive barrier for intrauterine adhesion.

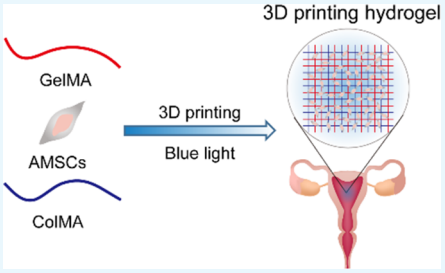

1. INTRODUCTION

Intrauterine adhesion (IUA) is known as Asherman syndrome and refers to damage of the basal layer of the endometrium caused by artificial abortion, curettage, and other factors, resulting in local or complete adhesion of the uterine cavity and the cervical canal.[1−3] A small amount of menstruation, recurrent abortion, and amenorrhea are major clinical manifestations, which seriously harm the reproductive health of females.[4] With the development of hysteroscopy technology, hysteroscopic electroresection of adhesions with minimally invasive, safe, and effective treatments has become the preferred choice for the treatment of IUA.[5] However, after postoperative wound exudation, infection, and other factors, the recurrence rate of secondary IUA is still very high. Therefore, after hysteroscopic electroresection of adhesions, enhancing endometrial repair and preventing readhesion remain the focus of the current treatment of IUA.[6] Development of an effective prevention strategy is a major challenge to intrauterine adhesion.

Recently, stem cell therapy has become a new method for the treatment of tissue injury and fibrosis, which has attracted much attention as a new and effective method for promoting the repair and regeneration of the endometrium.[7] Prior studies have shown that bone marrow-derived hematopoietic stem cell (BMDSC) transplantation can improve the fertility of IUA model mice, which can repair a damaged endometrium.[8] Previous research has shown that BMDSCs can differentiate into endometrial tissues in vivo.[9] Li et al. have found that human menstrual blood-derived mesenchymal stem cells (hEnSCs) can repair a damaged endometrium, induce angiogenesis, and enhance the fertility of endometrial damaged mice.[10] Zhao et al. found that adipose-derived stem cells (ADSCs) can promote the regeneration of endometrial cells and muscle cells and angiogenesis, resulting in achieving a better pregnancy outcome by transplanting cells to a locally resected uterus.[11] Zheng et al. found that human umbilical cord-derived mesenchymal stem cells (hUC-MSCs) may play a therapeutic role in chronic endometrial injury in rats by inhibiting excessive fibrosis and inflammation and enhancing endometrial cell proliferation and vascular remodeling.[12] Human amnion mesenchymal stem cells (hAMSCs) obtained

Received: April 21, 2021
Accepted: June 29, 2021
Published: September 3, 2021

https://doi.org/10.1021/acsomega.1c02117
ACS Omega 2021, 6, 23067−23075

from a human amniotic membrane are easily available and abundant, which have self-replication and multidirectional differentiation potential.[13] The cytokines secreted by hAMSCs have the effects of anti-inflammation and antifibrosis, promoting angiogenesis and promoting cell growth, and are expected to become a new treatment way for uterine adhesion.[14] Previous studies have shown that hAMSCs can contribute to the repair of the endometrium in rats, which proves the effectiveness of hAMSC transplantation in improving IUA.[15] However, the question of how to effectively transplant hAMSCs into the uterine cavity, retain its cell activity, and promote endometrial repair remains to be addressed.

Recently, a variety of physical films (electrospun fiber films, hydrogels, and sponges) have been used as barriers to minimize the complex process of adhesion formation.[16,17] However, the traditional tissue engineering membrane still has many shortcomings, such as a low cell implantation rate, a low matching degree between the membrane and tissue defects, and inaccurate localization of many kinds of cells. 3D printing technology can accurately control the material in time and space from the bottom forming unit and can also carry out personalized manufacturing according to the tissue defect site to achieve better tissue repair.[18] Moreover, 3D printing hydrogels based on cross-linking polymers have attracted wide attention because of their excellent biological and physical properties, such as excellent biocompatibility, high cell encapsulation efficiency, an in situ cross-linking ability, and controllable mechanical, swelling, and degradation properties.[19] Currently, hydrogels based on natural materials such as chitosan, gelatin, and hyaluronic acid have been used to prevent adhesion.[20−22] Due to their poor mechanical properties and rapid degradation, they are not yet able to achieve satisfactory treatment outcomes. In order to improve the physical properties of natural polymers and enhance their resistance to enzyme attacks,[23] light-activated materials play an increasingly important role in three-dimensional (3D) bioprinting technology. Prior research suggests that a GelMA hydrogel has good biological and adjustable physical properties, which allows cell proliferation and diffusion in GelMA hydrogel-based materials.[22,24] Collagen is the main component of the extracellular matrix (ECM), which is widely used in the field of biomaterials because of its good physical and chemical properties.[25−27] However, a pure collagen hydrogel has a single structure, simple properties, and poor mechanical properties.[28] Composite materials can have simultaneous advantages of both and avoid their own defects.

In this work, an effective and safe hydrogel for uterine adhesion prevention was developed by using 3D printing technology to encapsulate hAMSCs. Based on two natural biopolymers, gelatin (Gel) and collagen (Col) with high biocompatibility and biodegradability, GelMA and ColMA polymers were synthesized. Through using blue light to initiate a cross-linking reaction, a stable 3D printing hydrogel was prepared under mild conditions, which overcame the deficiency of UV light cross-linking leading to lower cell proliferation and viability. The swelling, rheological, and mechanical properties of the antiadhesion 3D printing hydrogel were studied. In addition, the biocompatibility and in vitro degradation were evaluated. Then, the cell release performance of the 3D printing hydrogel was further studied by stem cell encapsulation experiments in vitro. Finally, the anticavity adhesion efficacy of the 3D printing hydrogel was further evaluated in vivo in a rat IUA model.

2. RESULTS AND DISCUSSION

2.1. Material Synthesis. To obtain a photopolymerizable material, we chemically modified gelatin and collagen by nucleophilic substitution of carbonyl groups on methacrylic anhydride (MA) with nitrogen atoms on amino groups of gelatin or collagen. The reaction diagram and ^{1}H NMR spectra of the reaction products are shown in Figure 1A,B. The ^{1}H NMR spectra of GelMA and ColMA had two peaks at 5.4 and 5.89 ppm compared with the unmodified gelatin and collagen, representing the hydrogen absorption peak of methacryloyl, indicating that the methacrylic group was successfully grafted onto the molecular backbone of gelatin and collagen. According to the ratio of the integral area of the methacrylate proton integral to the methyl hydrogens of GelMA and ColMA, it can be calculated that the graft ratios of GelMA and ColMA are 59.6 and 36.7%, respectively.

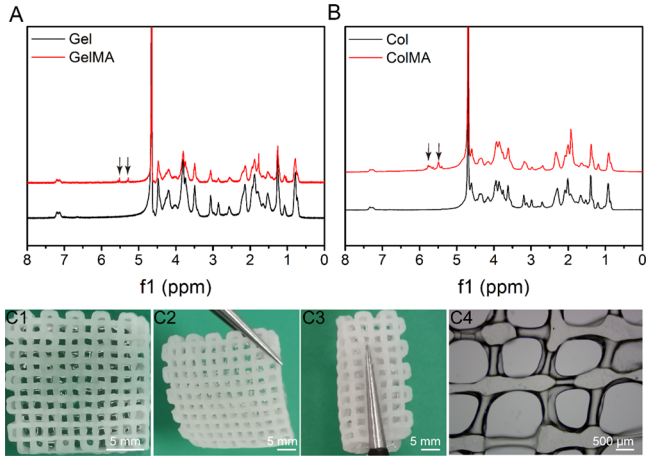

Figure 1. (A) ^{1}H NMR spectra of Gel and GelMA. (B) ^{1}H NMR spectra of Col and ColMA. Macroscopic appearance of the printed porous GelMA/ColMA hydrogel (C1−C4). 3D printed GelMA/ColMA hydrogel showing excellent mechanical performances: supporting its own weight (C2) and twisting (C3).

2.2. Characterization of the 3D Printed Hydrogel. Using an extruded 3D biological printer, we successfully printed a biological construct with a diameter of 14 mm and a height of 2 mm (Figure 1C1). It can be seen that the GelMA/ColMA hydrogel has good structural fidelity and can be stably cross-linked after being irradiated by blue light for 10 s. The 3D printed scaffolds showed excellent mechanical performances: supporting its own weight (Figure 1C2) and twisting (Figure 1C3). As shown in Figure 1C4, the filament diameter of the GelMA/ColMA hydrogel is 100 μm. It is worth mentioning that in the process of three-dimensional printing, the thickness of a water-solidified wire is affected by many parameters, such as temperature, air pressure, needle aperture, printing head moving speed, and so on. We stabilize the printed wire at a higher resolution by adjusting different parameters.

2.3. Swelling Analysis. The swelling ratio of each hydrogel was evaluated by the gravimetric method. The swelling phenomenon of a hydrogel in PBS is actually due to the diffusion of water molecules in PBS into the polymer of the hydrogel, and then, the molecular chain segment gradually extends and increases in the hydrogel through the interaction between water molecules and hydrogel molecular chains and finally shows the increase in polymer volume and mass macroscopically. As shown in Figure 2B, the measured swelling

https://doi.org/10.1021/acsomega.1c02117
ACS Omega 2021, 6, 23067−23075

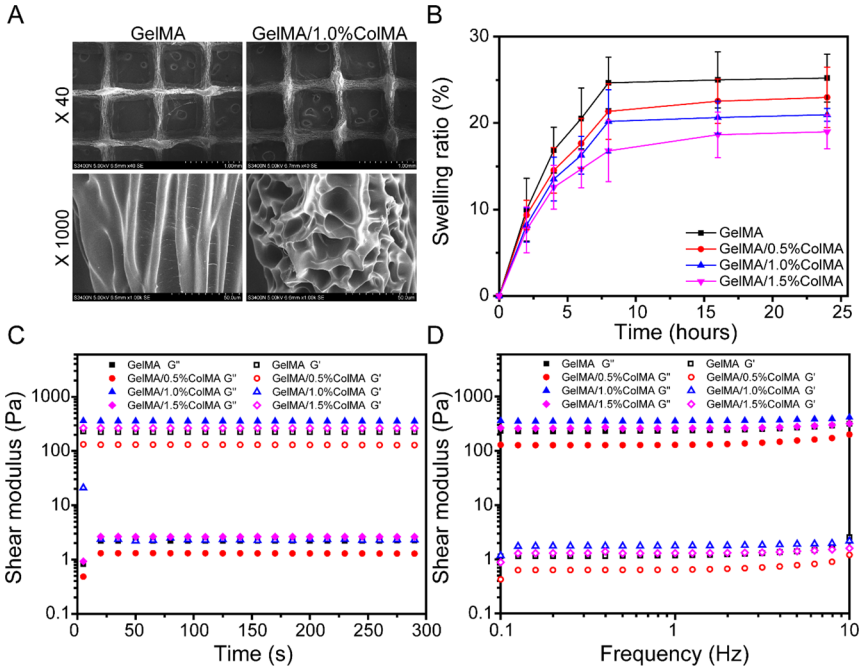

Figure 2. (A) SEM images of the printed porous GelMA and GelMA/ColMA hydrogels. (B) Swelling ratios of hydrogels. (C) Rheological properties. (D) Hydrogel viscosity with frequency ranging from 0.1 to 10 Hz.

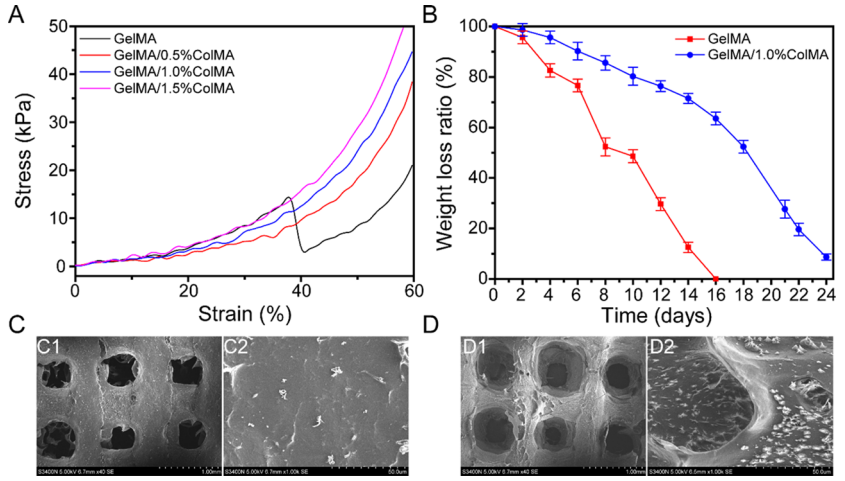

Figure 3. (A) Compressibility of hydrogels. (B) Weight loss rate of antiadhesion printed hydrogels in PBS solution containing a 1000 U/mL lysozyme. SEM images of the surface morphology of printed porous GelMA hydrogel (C) and GelMA/1.0%ColMA hydrogel (D) at day 8.

ratios for GelMA, GelMA/0.5%ColMA, GelMA/1.0%ColMA, and GelMA/1.5%ColMA were 25.2, 22.9, 20.9, and 19.0%, respectively. With the increase in ColMA concentration, the swelling ratio of the hydrogel decreased gradually. The slightly lower swelling ratio in GelMA/ColMA was due to the existence of ColMA increasing the cross-linking degree of composite hydrogels compared with pure GelMA hydrogels, which leads to the reduction of porosity. However, a low swelling ratio is still beneficial to prevent the swelling of the material from causing organ damage.

2.4. Rheological Properties. Rheological tests were performed to characterize the viscoelastic properties of hydrogels. As shown in Figure 2C, the storage modulus of the GelMA/ColMA hydrogel increases with the increase in ColMA concentration, indicating that the cross-linking degree between GelMA and ColMA increases. As shown in Figure 2D, the frequency dependence of the G' and G'' confirmed hydrogel-like behavior as G' is higher than G'' with the shear frequency from 0.1 to 10 rad/s, indicating that the hydrogels are stable and exhibit good mechanical properties.

2.5. Compression Modulus. An ideal material for intrauterine adhesion prevention should be equipped with suitable mechanical properties to remain its integrity during use. Gelatin and collagen are suitable biomaterials as they are biocompatible, biodegradable, and easy to manufacture, which have been widely used in tissue regeneration.[29,30] As shown in Figure 3A, the measured compression moduli for GelMA, GelMA/0.5% ColMA, GelMA/1.0%ColMA, and GelMA/1.5%ColMA were 24.7 ± 7.7, 40.0 ± 1.7, 43.63 ± 2.9, and 50.1 ± 3.5 kPa, respectively. It was shown that the compression modulus increased with increasing ColMA concentration when the GelMA concentration was fixed, which was due to a more compact structure within the GelMA/ColMA hydrogel. The compressibility of the GelMA/ColMA hydrogel increased with

https://doi.org/10.1021/acsomega.1c02117
ACS Omega 2021, 6, 23067−23075

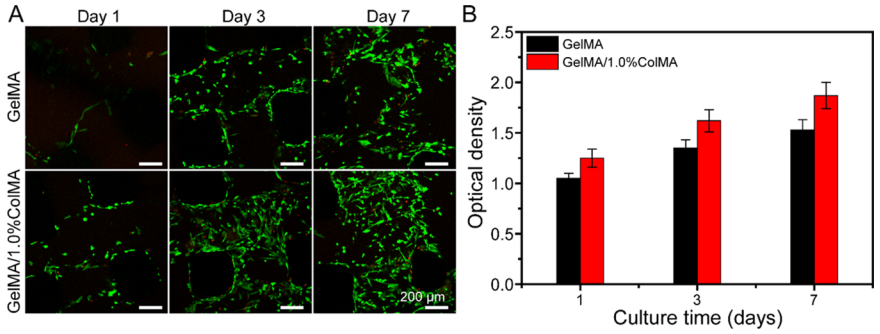

Figure 4. (A) Live/Dead staining images of hAMSCs cultured in the printed GelMA and GelMA/1.0%ColMA hydrogels at day 1, day 3, and day 7. Green fluorescence indicates living cells, and red fluorescence represents dead cells. (B) Proliferation of hAMSCs in the printed GelMA and GelMA/1.0%ColMA hydrogels by CCK-8 assay at day 1, day 3, and day 7.

the maximum strain reaching ∼60% compared to ∼35% in the GelMA hydrogel. A prior study reported that the compression modulus of a collagen scaffold used in a wounded rat uterus was 62.86 ± 6.23 kPa.[31] Our results indicated that the compression moduli of GelMA/1.0ColMA and GelMA/1.5%ColMA hydrogels were similar to the collagen scaffold, which had a good elasticity. Considering that the high compression modulus may cause extrusion to the uterus, the GelMA/1.0ColMA hydrogel is more suitable for application to intrauterine adhesion prevention.

2.6. In Vitro Degradation Study. An ideal and most useful antiadhesion material should have a degradation rate that matches the formation rate of injured tissue healing. As shown in Figure 3B, the GelMA hydrogel exhibited the fastest degradation rate and totally degraded after 16 days, which was very unfavorable to the repair of tissues in vivo. However, the degradation rate of the GelMA/ColMA hydrogel group reached 63.54% of the weight after 16 days, which is very much in line with the requirements of the adhesive tissue in terms of material degradation.[32,33] The results show that the GelMA/ColMA hydrogel group can maintain its relative integrity and stability during the degrading procedure in vitro, which accords with the standard of a material as a "physical barrier".[25] As shown in Figure 3C,D, some tiny pores began to appear on the surface of the hydrogel after 8 days but still maintained its structural integrity. In clinical uterine surgery, medical antiadhesion materials generally need to stay in the body for at least one week, so the GelMA/ColMA hydrogel is basically suitable for the antiadhesion effect in the uterus.

2.7. Biocompatible of Cells in the Hydrogel. In order to verify the biocompatibility of the hydrogel, we seeded stem cells on two types of hydrogels, namely, one was printed using 8% GelMA and the other was printed using GelMA/1.0%ColMA. To further observe the activity of cells on the hydrogels after the addition of ColMA, the cells on the hydrogels were observed by live/dead staining (green fluorescence indicates living cells, and red fluorescence represents dead cells). As shown in Figure 4A, most of the cells were alive in GelMA and GelMA/ColMA hydrogel groups and exhibited no obvious dead cells with time in culture. At day 1, stem cells were attached to all hydrogels, which showed similar morphology. After 3 and 7 days of culture, the stem cells grew freely, and the cell density increased gradually. It is worth noting that the cell density increased significantly in the GelMA/ColMA hydrogel group. The results showed that the GelMA/ColMA hydrogel had good biocompatibility, which was beneficial to the growth and proliferation of stem cells. As shown in Figure 4B, stem cells seeded on GelMA and GelMA/ColMA groups maintained a high proliferation rate during the culture period, indicating that cells can adhere to and proliferate on hydrogels. This is mainly because gelatin itself can promote cell adhesion and proliferation.[34] At day 7, the OD value of the GelMA/ColMA hydrogel increased significantly, indicating that the addition of ColMA can better support cell proliferation and growth, which was consistent with the results of live/dead staining. This is mainly due to the good biocompatibility of collagen and the highly porous structure of the hydrogel, which can promote cell proliferation.[35,36]

2.8. Morphology Analysis of hAMSCs. As shown in Figure 5, hAMSCs maintain high viability and are uniformly

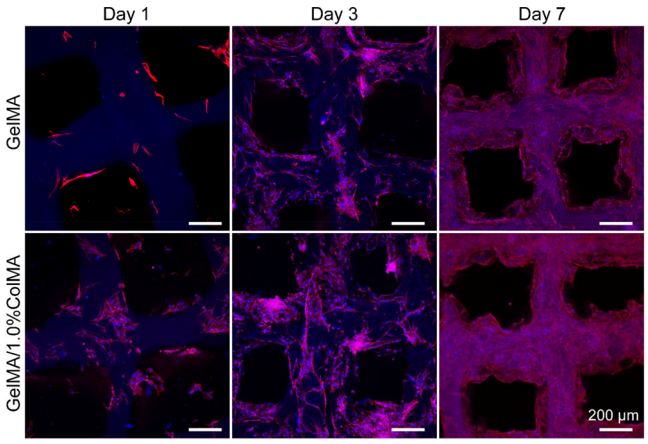

Figure 5. Cell morphology of hAMSCs in the printed GelMA and GelMA/1.0%ColMA hydrogels. Blue and red fluorescence represents the nucleus and actin filaments, respectively.

distributed inside the predefined 3D circular microchannels, which were further confirmed by cytoskeleton staining of the hAMSC monolayer. It can be seen that hAMSCs seeded on the channel surface formed a confluent monolayer and maintained their normal cellular phenotype, with normal expression of F-actin and the nucleus. In addition, it was noticeable that the morphology of hAMSCs grown on the GelMA/1.0%ColMA hydrogel was different from that on the pure GelMA hydrogel, which exhibited more elongation and thicker actin filaments.

2.9. Cell Delivery Properties of the GelMA/ColMA Hydrogel. hAMSCs have been shown to have the ability to repair the endometrium, which is promising in preventing postsurgical peritoneal adhesion.[37] Therefore, we selected hAMSCs to test the cell delivery capacity of hydrogels. The cells were tested for 7 days, and the cell release was monitored.

https://doi.org/10.1021/acsomega.1c02117
ACS Omega 2021, 6, 23067−23075

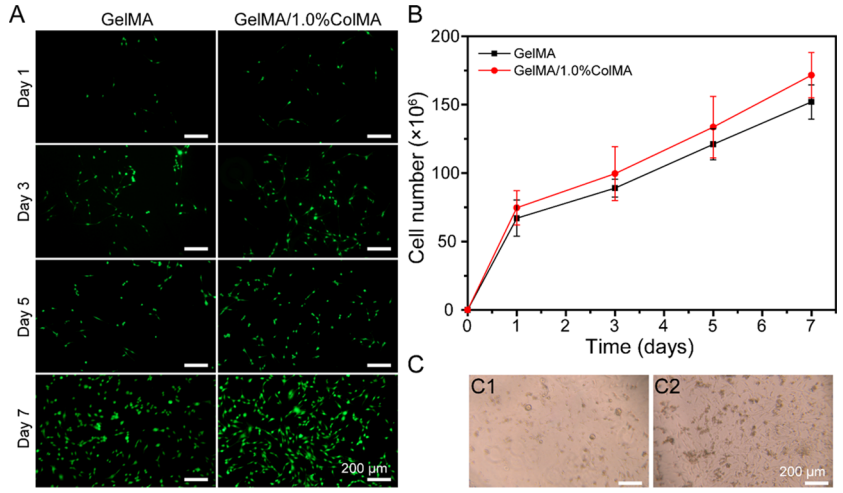

Figure 6. (A) Live/Dead staining images of delivered cells in the printed GelMA and GelMA/1.0%ColMA hydrogels at days 1, 3, 5, and 7. Green fluorescence indicates living cells, and red fluorescence represents dead cells. Scale bar = 200 μm. (B) Cumulative delivery profiles of hAMSCs inside the printed GelMA and GelMA/1.0%ColMA hydrogels at days 1, 3, 5, and 7. (C) Morphology of released hAMSCs from GelMA and GelMA/1.0% ColMA hydrogels at day 7. Scale bar = 200 μm. Each group includes three experimental repeats.

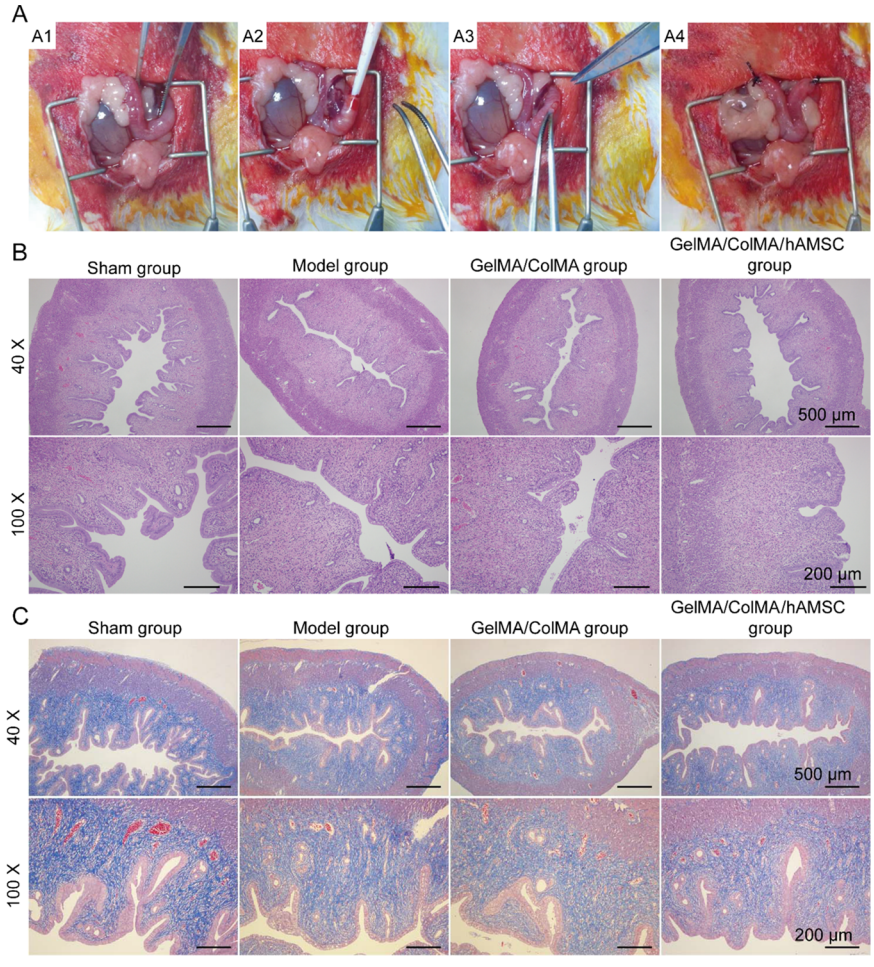

Figure 7. (A) Photographs of the used hydrogels and the process of the surgery. A1, Opening the abdomen; A2, scratching the endometrial tissue; A3, placing the 3D printing GelMA/ColMA/hAMSC hydrogel inside the uterus; A4, suturing the uterus. (B) Representative H&E staining images of cavity adhesion in the rat IUA model. The nucleus was blue, while muscle fibers and the cytoplasm were red. (C) Representative Masson staining images of cavity adhesion in the rat IUA model.

As shown in Figure 6A, it was clear that most of the released HAMSCs were alive. As shown in Figure 6B, the HAMSC release curve shows a cumulative increasing monotonic trend, which implies that these hydrogels can provide a stable cell supply to tissue repair. As shown in Figure 6C, the released hAMSCs inside the GelMA/1.0%ColMA hydrogel network at

https://doi.org/10.1021/acsomega.1c02117
ACS Omega 2021, 6, 23067−23075

day 7 show normal cell morphology, indicating that the cell function has been restored when the cell is released from the encapsulated 3D printing GelMA/1.0%ColMA hydrogel.

2.10. In Vivo Antiadhesion of the GelMA/ColMA/hAMSC Hydrogel in the Rat IUA Model. The photographs of the used hydrogels and the process of the surgery are shown in Figure 7A. After placing the 3D printing GelMA/ColMA/hAMSC hydrogel inside the uterus and suturing the uterus, there was no redness and swelling reaction in the uterus, which indicated that the 3D printing hydrogel has no side effects on the uterus. As shown in Figure 7B, the shapes of the uterine cavity and the endometrial gland were normal in the sham operation group. However, the uterine cavity had partial atresia, intimal atrophied, and the number of glands decreased in the model group, which indicated that the IUA model was successfully established. Compared to the model group, the hysteric cavity in the GelMA/ColMA hydrogel group is closed, and the degree of intimal atrophy was mild. A prior study reported that 3D printing hydrogels could prevent postsurgical peritoneal adhesion.[38] Compared to the model group, the uterine cavity in the GelMA/ColMA/hAMSC hydrogel group is large, and there was no atrophy of the endometrium. Meanwhile, the recovery effect of the GelMA/ColMA/hAMSC hydrogel group was basically consistent with the sham operation group. As shown in Figure 7C, substantial collagen fiber deposition was observed in the model group, which indicated that the model was established successfully. Meanwhile, the percentage of the fibrotic area was significantly lower in the GelMA/ColMA/hAMSC hydrogel group compared to that of the model group. A prior study indicated that hAMSCs could have the potential of endometrial cell differentiation and promote rat endometrial repair.[15] All results indicated that the GelMA/ColMA/hAMSC hydrogel has a superior antiadhesion capability in the rat IUA model.

3. MATERIALS AND METHODS

3.1. Materials. Gelatin (Gel, BioReagent, from cold water fish skin) was purchased from Sigma-Aldrich Co., Ltd. (Darmstadt, Germany). Collagen (Col, type I collagen, MW = 100−200 kDa) was obtained from Haishen Biotechnology Co., Ltd. (Fuzhou, China). Methacrylic anhydride (MA) was purchased from Maclean Biochemical Technology Co., Ltd. (Shanghai, China). A photoinitiator (lithium phenyl-2,4,6-trimethylbenzoylphosphinate, LAP) was purchased from Shanghai Yingchang Biotechnology Co., Ltd. (Shanghai, China). Cell Counting Kit-8 (CCK-8) and Live/Dead cell staining kits were purchased from BestBio Co., Ltd. (Shanghai, China). TRITC phalloidin and 4,6-diamidino-2-phenylindole (DAPI) were obtained from Biyuntian Biotechnology Co., Ltd. (Shanghai, China). Human amnion mesenchymal stem cells (hAMSCs) derived from a human amnion were purchased from Fuyuan Biotechnology Co., Ltd. (Shanghai, China). Unless otherwise stated, all chemicals were of analytical reagent grade.

3.2. Synthesis of Methylacrylated Gelatin (GelMA). GelMA was synthesized according to a previous report.[39] In brief, 10 g of gelatin was dissolved in 100 mL of deionized water at 50 °C to make a 10% w/v homogeneous solution. Then, 0.6 mL of methacrylic anhydride (MA) per gram of gelatin was added dropwise into the gelatin solution, and the solution was stirred for 6 h. The reaction solution was dialyzed in deionized water for 3 days using a 12−14 kDa dialysis tubing to remove the impurities and methacrylic acid. The solution was then freeze-dried, protected from light, and stored at −80 °C until further use.

3.3. Synthesis of Methylacrylated Collagen (ColMA). Collagen was modified with methacrylic groups based on a method as described previously.[40] In brief, 2 g of collagen was dissolved in 100 mL of deionized water at 37 °C to make a 2% w/v homogeneous solution. Then, 1.2 mL of methacrylic anhydride (MA) was added dropwise into the collagen solution, and the solution was stirred for 12 h. The pH of the mixed solution was maintained between 8 and 9 using 5 M NaOH. The reaction solution was dialyzed in deionized water using a 12−14 kDa dialysis tubing for 3 days with the dialysate being refreshed three times daily. The final dialyzed product was then freeze-dried, protected from light, and stored at −20 °C until further use. ^{1}H NMR spectra were taken using a 500 MHz NMR spectrophotometer (Bruker, Rheinstetten, Germany).

3.4. Preparation of GelMA/ColMA Composite Hydrogels. For precursors of the GelMA/ColMA hydrogel, the freeze-dried GelMA foams and ColMA foams were dissolved in PBS solution. The final precursors were composed of 8% GelMA, 8% GelMA + 0.5% ColMA, 8% GelMA + 1.0% ColMA, and 8% GelMA + 1.5% ColMA. The 0.1% (w/v) photoinitiator LAP was added into the pregel solutions and were then covalently cross-linked through blue light irradiation (wavelength = 405 nm, intensity ≈ 1 mW/cm^2).

3.5. Rheological Characterization. Dynamic rheological experiments were measured using a TA rheometer instrument (Kinexus, Ma Erwen Instruments, Britain) equipped with a plate with a diameter of 20 mm and a 0.5 mm gap. To measure the stiffness, hydrogels were measured by a time sweep test at a 1% strain and a 1 Hz frequency for 600 s at 25 °C. To measure the storage modulus (G') and loss modulus (G''), hydrogels were measured by a frequency sweep test with a constant strain of 0.5% and changing the frequency from 0.1 to 10 Hz at 25 °C.

3.6. Compression Tests. For compression tests of hydrogels, the samples were prepared into cylinders (11 mm in diameter and 8 mm in height) and measured using a universal testing machine (ELF3200; Bose, America). The crosshead speed was set at 0.05 mm/s. The compressive moduli were calculated from a strain of 60% in the stress−strain curve.

3.7. Measurement of Dynamic Swelling Behavior of Hydrogels. The swelling ability of the hydrogels was measured using a conventional gravimetric method. Test hydrogels were weighed to record their initial wet weights and then separately immersed in PBS at 37 °C. At specified time intervals (t = 2, 4, 6, 8, 16, and 24 h), PBS on the surface of each sample was gently blotted followed by weighting the swollen wet mass. The swelling ratio of the hydrogels was calculated according to the following formula

$$\text{Swelling ratio} = \frac{W_t - W_i}{W_i}$$

where "W_i" and "W_t" are the weight of the initial hydrogel and the swollen hydrogels at time t (t is the time that the hydrogel was immersed in distilled water), respectively.

3.8. Morphological Examination. The printed strands, pore sizes, and the top-section morphologies of the freeze-dried 3D printed hydrogels were observed using a scanning electron microscope (SEM; EVO MA 15/LS 15, Carl Zeiss, Germany). The lyophilized samples were coated with gold using a sputter coater for 30 s and observed under an accelerating voltage of 5 kV.

https://doi.org/10.1021/acsomega.1c02117
ACS Omega 2021, 6, 23067−23075

3.9. In Vitro Degradation Test. To mimic the in vivo microenvironment, the biodegradation behavior of hydrogels was evaluated in enzymatic degradation experiments. The 3D printed hydrogel samples were immersed in PBS (0.01 M, pH = 7.4) containing a 1000 U/mL lysozyme with constant shaking (50 rpm) at 37 °C. After predetermined time intervals, the samples were carefully taken out and rinsed with deionized water for 5 times then lyophilized and weighted. The degradation rate was calculated according to the following formula

$$\text{Degradation ratio} = \frac{M_0 - M_t}{M_0} \times 100\%$$

where "M_0" and "M_t" are the weight of the initial hydrogel and the hydrogel after degradation at a certain time interval, respectively.

3.10. 3D Bioprinting Hydrogel. A commercial 3D printer (EFL-BP-6800, Suzhou Intelligent Manufacturing Research Institute, Suzhou, China) was used to print the 3D hydrogel constructs. Before printing, we designed a layer-by-layer lattice structure (16 mm × 16 mm, 2 layers). During printing, the fiber diameter was 100 μm, the printing speed was 20 mm/s, the temperature of the base plate was 4 °C, and the nozzle temperature was 20 °C. After the printing process, 3D hydrogels were blue light-cross-linked for 10 s.

3.11. In Vitro Biocompatibility Characterization. Human amnion mesenchymal stem cells (hAMSCs) were cultured in the fresh Dulbecco modified Eagle medium (DMEM) supplemented with 10% fetal bovine serum (FBS), 1% penicillin (100 units/mL), and streptomycin (100 μg/mL). Cells were propagated in a 175 cm^2 tissue culture flask and incubated at 37 °C in 5% CO_2. The media were refreshed every other day, and cells were passaged every 4 to 7 days with 0.25% trypsin and 1% EDTA. An hAMSC cell suspension with a density of 2 × 10^4 cells/mL was added to the surface of the sterilized 3D printed hydrogel (one hydrogel in each well of 24-well plates). The cell-seeded hydrogels were incubated at 37 °C in 5% CO_2, and the media were refreshed every other day. After being cultured for 1 day, 3 days, and 7 days, samples were then washed three times with PBS. The viability and proliferation were assessed using the Live/Dead staining and Cell Counting Kit-8 (CCK-8) according to the manufacturer's instructions.

Live and dead cells on the surface of 3D printed hydrogels were visualized using the Live/Dead assay kit according to the manufacturer's protocol. After cell implantation, the hydrogels were gently rinsed with 1× PBS for 3 times and then immersed in a Live/Dead working solution (2 μM calcein AM, 8 μM PI) at 37 °C for 45 min in the dark. Subsequently, the 3D constructs were rinsed with 1× PBS for 1 time and added with the fluorescence-quenching agent. Finally, the cells on 3D printed hydrogels were observed by laser scanning confocal microscopy (Olympus FV3000, Tokyo, Japan). Viable cells (green fluorescence) were stained with calcein AM, whereas dead cells (red fluorescence) were stained with PI.

For CCK-8 colorimetric assay, 50 μL of a CCK8 solution and 1450 μL of DMEM media were added to each well, and the cells were further incubated in an incubator for 3 h. Finally, the final solutions were transferred to a 96-well plate (200 μL per well) to measure the OD values at 450 nm using a microplate reader (Molecular Devices, Sunnyvale, CA).

3.12. Cytoskeleton Immunofluorescence Staining. Cytoskeletons in the 3D printed hydrogels were visualized using TRITC phalloidin and DAPI according to the manufacturer's protocol. Briefly, the 3D printed hydrogels were fixed in 4% paraformaldehyde for 30 min, washed three times with 1× PBS, soaked in 0.5% Triton X-100 for 10 min, and washed 3 times with 1× PBS. Next, the samples were incubated in 4 μg/mL TRITC phalloidin followed by PBS washes for 3 times. Nuclei were stained with 1 μg/mL DAPI solution in the dark for 15 min followed by PBS washes for three times and added with the fluorescence-quenching agent (G1401, Servicebio Co., Ltd., China) at 4 °C protected from light. Finally, the images were acquired by laser scanning confocal microscopy (FV 3000, Olympus, Japan). The cytoskeleton (red fluorescence) was stained with TRITC phalloidin, and the cellular nuclei (blue fluorescence) were stained with DAPI.

3.13. In Vitro Cell Delivery Property of the 3D Printed Hydrogels. First, GelMA and GelMA/ColMA hydrogels containing hAMSCs (1 × 10^7 cells/mL) were 3D printed. Then, hydrogels were placed in 24-well plates, and 1.5 mL of DMEM with 10% FBS was added into each well. At various time points, the released cell survival and the number in hydrogels were measured using the Live/Dead cell kit and a Countess II FL automated cell counter (Life Technologies, Carlsbad, CA, USA). Meanwhile, the released cells were observed using an optical microscope (Shanghai Optical Instrument Factory, Shanghai, China) at day 7.

3.14. Establishment of the Intrauterine Adhesion (IUA) Model. All animal experiments were approved by the Jinan University Institutional Animal Care and Use Committee. The scratching method was used to construct the IUA model as described previously with slight modifications.[41] The rats were examined for an estrous cycle by vaginal smear tests. Under an aseptic environment, rats were anesthetized with pentobarbital (45 mg/kg), and their abdomen was disinfected with iodine. A 3−4 cm longitudinal incision was made along the abdominal white line to enter the abdominal cavity, separate the tissue, and confirm the location of the uterus. Taking the right uterine horn, a 2 mm diameter incision was crosscut at the junction of the uterine body and the uterine horn about 1 cm. Then, the endometrial tissue was scratched up and down by a curette with a diameter of 2 mm. The length of the uterine injury is about 3−4 cm. To prevent scratching through the myometrium, the curettage is stopped when the uterine wall is thin and translucent. The left uterine horn is treated with the same method. The abdominal cavity was rinsed with normal saline, and the abdomen was closed layer by layer. The rats were subdivided into 4 groups: (1) the sham operation group (sham group, n = 3), where the abdomen was opened and the abdominal cavity was exposed about, the abdomen was closed layer by layer after 15 min, and the uterus was not treated; (2) the PBS model group (model group, n = 3), where the IUA model was built according to the above method and the rats were injected with 10 μL of PBS in each of the two uterine horns; (3) the GelMA/ColMA hydrogel-treated group (GelMA/ColMA group, n = 3), where the rats were placed with the 3D printed GelMA/ColMA hydrogel in each of the two uterine horns; (4) the GelMA/ColMA/hAMSC hydrogel-treated group (GelMA/ColMA/hAMSC group, n = 3), where the rats were placed with the 3D printed GelMA/ColMA/hAMSC hydrogel in each of the two uterine horns.

Rats were sacrificed at day 14 post treatment, and the double-layer uterine tissue was collected. Uterine tissue samples were routinely fixed with 4% paraformaldehyde for 24 h, embedded in paraffin, and cut into sections with a thickness of 4 μm. Subsequently, sections were stained with hematoxylin and eosin

https://doi.org/10.1021/acsomega.1c02117
ACS Omega 2021, 6, 23067−23075

(H&E) according to the manufacturer's protocol. The stained sections were observed with a light microscope (RM2016, Leica, Shanghai, China).

3.15. Statistical Analysis. All determinations were performed at least in triplicate, and the results were expressed as means ± standard deviation (mean ± SD). Statistical comparisons were subjected to one-way ANOVA statistical analysis using SPSS 22.0 software (SPSS, Chicago, USA). Values of $*p < 0.05$, $**p < 0.01$, and $***p < 0.001$ were considered to demonstrate statistical significance.

4. CONCLUSIONS

A composite GelMA/ColMA hydrogel for intrauterine adhesion prevention was developed by using 3D printing technologies. The presented antiadhesion hydrogel has a porous 3D structure, improved mechanical properties, and prolonged degradability. The results of in vitro experiments demonstrated that stem cells can realize liable attachment and uniform spreading on the surface of the inner wall of the channels, showing high survival rates, normal proliferation rates, and good cell morphology. Moreover, in the 3D printed GelMA/ColMA hydrogel, stem cells were continuously released for at least 7 days in vitro. The results of in vivo experiments demonstrated that the GelMA/ColMA/hAMSC hydrogel has an antiadhesion capability in the rat IUA model. Furthermore, the finding of this work indicated that the 3D printed GelMA/ColMA hydrogel may offer a biocompatible, feasible, and efficient way for the study of tissue engineering development.

AUTHOR INFORMATION

Corresponding Authors

Rui Guo − *Key Laboratory of Biomaterials of Guangdong Higher Education Institutes, Guangdong Provincial Engineering and Technological Research Center for Drug Carrier Development, Department of Biomedical Engineering, Jinan University, Guangzhou 510632, P. R. China*; Email: guorui@jnu.edu.cn

Liwei Han − *Department of Gynecology, Family Planning Research Institute of Guangdong Province, Guangzhou 510600, P. R. China*; orcid.org/0000-0003-4896-7483; Email: hanliwei719@qq.com

Authors

Miao Feng − *NHC Key Laboratory of Male Reproduction and Genetics, Guangzhou 510600, P. R. China; Department of Gynecology, Family Planning Research Institute of Guangdong Province, Guangzhou 510600, P. R. China*

Shengxue Hu − *Beogene Biotech (Guangzhou) Co., Ltd., Guangzhou 510663, P. R. China*

Weibing Qin − *NHC Key Laboratory of Male Reproduction and Genetics, Guangzhou 510600, P. R. China; Department of Center Laboratory, Family Planning Research Institute of Guangdong Province, Guangzhou 510600, P. R. China*

Yunge Tang − *NHC Key Laboratory of Male Reproduction and Genetics, Guangzhou 510600, P. R. China; Department of Center Laboratory, Family Planning Research Institute of Guangdong Province, Guangzhou 510600, P. R. China*

Complete contact information is available at: https://pubs.acs.org/10.1021/acsomega.1c02117

Author Contributions

#M.F. and S.H. contributed equally to this work.

Notes

The authors declare no competing financial interest.

ACKNOWLEDGMENTS

This work was supported by the Fund of the NHC Key Laboratory of Male Reproduction and Genetics (no. KF201705).

REFERENCES

(1) Wei, C.; Pan, Y.; Zhang, Y.; Dai, Y.; Jiang, L.; Shi, L.; Yang, W.; Xu, S.; Zhang, Y.; Xu, W.; Zhang, Y.; Lin, X.; Zhang, S. Overactivated sonic hedgehog signaling aggravates intrauterine adhesion via inhibiting autophagy in endometrial stromal cells. *Cell Death Dis.* **2020**, *11*, 755−755.

(2) Zhu, X.; Ye, H.; Fu, Y. The effect of frozen-thawed embryo transfer performed concurrently with hysteroscopy on the reproductive outcomes during assisted reproductive treatments. *Sci. Rep.* **2017**, *7*, 11852−11852.

(3) Chen, G.; Liu, L.; Sun, J.; Zeng, L.; Cai, H.; He, Y. Foxf2 and Smad6 co-regulation of collagen 5A2 transcription is involved in the pathogenesis of intrauterine adhesion. *J. Cell Mol. Med.* **2020**, *24*, 2802−2818.

(4) Guo, L.-P.; Chen, L.-M.; Chen, F.; Jiang, N.-H.; Sui, L. Smad signaling coincides with epithelial-mesenchymal transition in a rat model of intrauterine adhesion. *Am. J. Transl. Res.* **2019**, *11*, 4726−4737.

(5) Sebbag, L.; Even, M.; Fay, S.; Naoura, I.; Revaux, A.; Carbonnel, M.; Pirtea, P.; de Ziegler, D.; Ayoubi, J.-M. Early Second-Look Hysteroscopy: Prevention and Treatment of Intrauterine Post-surgical Adhesions. *Front. Surg.* **2019**, *6*, 50.

(6) Zhang, S.-S.; Xia, W.-T.; Xu, J.; Xu, H.-L.; Lu, C.-T.; Zhao, Y.-Z.; Wu, X.-Q. Three-dimensional structure micelles of heparin-poloxamer improve the therapeutic effect of 17β-estradiol on endometrial regeneration for intrauterine adhesions in a rat model. *Int. J. Nanomed.* **2017**, *Volume 12*, 5643−5657.

(7) Xin, L.; Lin, X.; Pan, Y.; Zheng, X.; Shi, L.; Zhang, Y.; Ma, L.; Gao, C.; Zhang, S. A collagen scaffold loaded with human umbilical cord-derived mesenchymal stem cells facilitates endometrial regeneration and restores fertility. *Acta Biomater.* **2019**, *92*, 160−171.

(8) Gil-Sanchis, C.; Cervelló, I.; Khurana, S.; Faus, A.; Verfaillie, C.; Simón, C. Contribution of different bone marrow-derived cell types in endometrial regeneration using an irradiated murine model. *Fertil. Steril.* **2015**, *103*, 1596−1605.e1.

(9) Santamaria, X.; Mas, A.; Cervelló, I.; Taylor, H.; Simon, C. Uterine stem cells: from basic research to advanced cell therapies. *Hum. Reprod. Update* **2018**, *24*, 673−693.

(10) Li, H.; Yahaya, B. H.; Ng, W. H.; Yusoff, N. M.; Lin, J. Conditioned Medium of Human Menstrual Blood-Derived Endometrial Stem Cells Protects Against MPP-Induced Cytotoxicity *in vitro*. *Front. Mol. Neurosci.* **2019**, *12*, 80.

(11) Zhao, S.; Qi, W.; Zheng, J.; Tian, Y.; Qi, X.; Kong, D.; Zhang, J.; Huang, X. Exosomes Derived from Adipose Mesenchymal Stem Cells Restore Functional Endometrium in a Rat Model of Intrauterine Adhesions. *Reprod. Sci.* **2020**, *27*, 1266−1275.

(12) Zheng, J.-H.; Zhang, J.-K.; Kong, D.-S.; Song, Y.-B.; Zhao, S.-D.; Qi, W.-B.; Li, Y.-N.; Zhang, M.-l.; Huang, X.-H. Quantification of the CM-Dil-labeled human umbilical cord mesenchymal stem cells migrated to the dual injured uterus in SD rat. *Stem Cell Res. Ther.* **2020**, *11*, 280.

(13) Tang, Z.; Wu, X.; Hu, L.; Xiao, Y.; Tan, J.; Zuo, S.; Shen, M.; Yuan, X. Circ-100290 Positively Regulates Angiogenesis Induced by Conditioned Medium of Human Amnion-Derived Mesenchymal Stem Cells Through miR-449a/eNOS and miR-449a/VEGFA Axes. *Inter. J. Biol. Sci.* **2020**, *16*, 2131−2144.

(14) Li, B.; Zhang, Q.; Sun, J.; Lai, D. Human amniotic epithelial cells improve fertility in an intrauterine adhesion mouse model. *Stem Cell Res. Ther.* **2019**, *10*, 257.

(15) Gan, L.; Duan, H.; Xu, Q.; Tang, Y.-Q.; Li, J.-J.; Sun, F.-Q.; Wang, S. Human amniotic mesenchymal stromal cell transplantation improves endometrial regeneration in rodent models of intrauterine adhesions. *Cytotherapy* **2017**, *19*, 603−616.
(16) Yang, Y.; Zhao, X.; Yu, J.; Chen, X.; Chen, X.; Cui, C.; Zhang, J.; Zhang, Q.; Zhang, Y.; Wang, S.; Cheng, Y. H-Bonding Supramolecular Hydrogels with Promising Mechanical Strength and Shape Memory Properties for Postoperative Antiadhesion Application. *ACS Appl. Mater. Interfaces* **2020**, *12*, 34161−34169.
(17) Ohta, S.; Toda, T.; Inagaki, F.; Omichi, K.; Shimizu, A.; Kokudo, N.; Hasegawa, K.; Ito, T. The Prevention of Hepatectomy-Induced Adhesions by Bilayer Sponge Composed of Ultrapure Alginate. *J. Surg. Res.* **2019**, *242*, 286−295.
(18) Potyondy, T.; Uquillas, J.; Tebon, P.; Byambaa, B.; Hasan, A.; Tavafoghi, M.; Mary, H.; Aninwene Ii, G.; Pountos, I.; Khademhosseini, A.; Ashammakhi, N. Recent advances in 3D bioprinting of musculoskeletal tissues. *Biofabrication* **2021**, No. 022001.
(19) Zhang, P.; Wang, H.; Wang, P.; Zheng, Y.; Liu, L.; Hu, J.; Liu, Y.; Gao, Q.; He, Y. Lightweight 3D bioprinting with point by point photocuring. *Bioact. Mater.* **2021**, *6*, 1402−1412.
(20) Cheng, F.; Wu, Y.; Li, H.; Yan, T.; Wei, X.; Wu, G.; He, J.; Huang, Y. Biodegradable *N*, *O*-carboxymethyl chitosan/oxidized regenerated cellulose composite gauze as a barrier for preventing postoperative adhesion. *Carbohydr. Polym.* **2019**, *207*, 180−190.
(21) Feng, B.; Wang, S.; Hu, D.; Fu, W.; Wu, J.; Hong, H.; Domian, I. J.; Li, F.; Liu, J. Bioresorbable electrospun gelatin/polycaprolactone nanofibrous membrane as a barrier to prevent cardiac postoperative adhesion. *Acta Biomater.* **2019**, *83*, 211−220.
(22) Cheng, M.; Chang, W.-H.; Yang, S.-T.; Huang, H.-Y.; Tsui, K.-H.; Chang, C.-P.; Lee, W.-L.; Wang, P.-H. Efficacy of Applying Hyaluronic Acid Gels in the Primary Prevention of Intrauterine Adhesion after Hysteroscopic Myomectomy: A Meta-Analysis of Randomized Controlled Trials. *Life* **2020**, *10*, 285.
(23) Fierke, C. A.; Hammes, G. G. Transient kinetic approaches to enzyme mechanisms. In *Contemporary Enzyme Kinetics and Mechanism*; 2nd Ed.; Purich, D. Ed.; Academic Press: New York, 1996; pp. 1−35.
(24) Doe, J. S.; Smith, J.; Roe, P. Syntheses and biological activities of rebeccamycin analogues. Introduction of a halogenoacetyl substituent. *J. Am. Chem. Soc.* **1968**, *90*, 8234−8241.
(25) Cai, X.; Hu, S.; Yu, B.; Cai, Y.; Yang, J.; Li, F.; Zheng, Y.; Shi, X. Transglutaminase-catalyzed preparation of crosslinked carboxymethyl chitosan/carboxymethyl cellulose/collagen composite membrane for postsurgical peritoneal adhesion prevention. *Carbohydr. Polym.* **2018**, *201*, 201−210.
(26) Hu, S.; Cai, X.; Qu, X.; Yu, B.; Yan, C.; Yang, J.; Li, F.; Zheng, Y.; Shi, X. Preparation of biocompatible wound dressings with long-term antimicrobial activity through covalent bonding of antibiotic agents to natural polymers. *Int. J. Biol. Macromol.* **2019**, *123*, 1320−1330.
(27) Kurzyński, M. Protein machine model of enzymatic reactions gated by enzyme internal dynamics. *Biophys. Chem.* **1997**, *65*, 1−28.
(28) Chen, J.; Cai, Z.; Wei, Q.; Wang, D.; Wu, J.; Tan, Y.; Lu, J.; Ai, H. Proanthocyanidin-crosslinked collagen/konjac glucomannan hydrogel with improved mechanical properties and MRI trackable biodegradation for potential tissue engineering scaffolds. *J. Mater. Chem. B* **2020**, *8*, 316−331.
(29) Abbas, Y.; Brunel, L. G.; Hollinshead, M. S.; Fernando, R. C.; Gardner, L.; Duncan, I.; Moffett, A.; Best, S.; Turco, M. Y.; Burton, G. J.; Cameron, R. E. Generation of a three-dimensional collagen scaffold-based model of the human endometrium. *Interface Focus* **2020**, *10*, 20190079.
(30) Su, K.; Edwards, S. L.; Tan, K. S.; White, J. F.; Kandel, S.; Ramshaw, J. A. M.; Gargett, C. E.; Werkmeister, J. A. Induction of endometrial mesenchymal stem cells into tissue-forming cells suitable for fascial repair. *Acta Biomater.* **2014**, *10*, 5012−5020.
(31) Xiao, B.; Yang, W.; Lei, D.; Huang, J.; Yin, Y.; Zhu, Y.; You, Z.; Wang, F.; Sun, S. PGS Scaffolds Promote the In Vivo Survival and Directional Differentiation of Bone Marrow Mesenchymal Stem Cells Restoring the Morphology and Function of Wounded Rat Uterus. *Adv. Healthcare Mater.* **2019**, *8*, e1801455.
(32) Menzies, D.; Ellis, H. Intestinal obstruction from adhesions–how big is the problem? *Ann. R. Coll. Surg. Engl.* **1990**, *72*, 60−63.
(33) Wu, W.; Ni, Q.; Xiang, Y.; Dai, Y.; Jiang, S.; Wan, L.; Liu, X.; Cui, W. Fabrication of photo-crosslinked gelatin hydrogel for preventing abdominal adhesion. *RSC Adv.* **2016**, *6*, 92449−92453.
(34) Jin, X.; Shang, Y.; Zou, Y.; Xiao, M.; Huang, H.; Zhu, S.; Liu, N.; Li, J.; Wang, W.; Zhu, P. Injectable Hypoxia-Induced Conductive Hydrogel to Promote Diabetic Wound Healing. *ACS Appl. Mater. Interfaces* **2020**, *12*, 56681−56691.
(35) Ucar, B.; Kajtez, J.; Foidl, B. M.; Eigel, D.; Werner, C.; Long, K. R.; Emnéus, J.; Bizeau, J.; Lomora, M.; Pandit, A.; Newland, B.; Humpel, C. Biomaterial based strategies to reconstruct the nigrostriatal pathway in organotypic slice co-cultures. *Acta Biomater.* **2021**, *121*, 56681−56262.
(36) Dutta, S. D.; Hexiu, J.; Patel, D. K.; Ganguly, K.; Lim, K.-T. 3D-printed bioactive and biodegradable hydrogel scaffolds of alginate/gelatin/cellulose nanocrystals for tissue engineering. *Int. J. Biol. Macromol.* **2021**, *167*, 644−658.
(37) Yang, Y.; Mao, Y.; Wang, J.; Sun, C.; Zhang, Y.; Chen, X. In vivo tracing of human amniotic mesenchymal stem cells labeled with PKH26 in rat intrauterine adhesions model. *Shengwu Gongcheng Xuebao Chin. J. Biotechnol.* **2018**, *34*, 1660−1667.
(38) Cho, H.; Jammalamadaka, U.; Tappa, K.; Egbulefu, C.; Prior, J.; Tang, R.; Achilefu, S. 3D Printing of Poloxamer 407 Nanogel Discs and Their Applications in Adjuvant Ovarian Cancer Therapy. *Mol. Pharmaceutics* **2019**, *16*, 552−560.
(39) Zhou, F.; Hong, Y.; Zhang, X.; Yang, L.; Li, J.; Jiang, D.; Bunpetch, V.; Hu, Y.; Ouyang, H.; Zhang, S. Tough hydrogel with enhanced tissue integration and in situ forming capability for osteochondral defect repair. *Appl. Mater. Today* **2018**, *13*, 32−44.
(40) Eke, G.; Mangir, N.; Hasirci, N.; MacNeil, S.; Hasirci, V. Development of a UV crosslinked biodegradable hydrogel containing adipose derived stem cells to promote vascularization for skin wounds and tissue engineering. *Biomaterials* **2017**, *129*, 188−198.
(41) Zhao, Y.-x.; Chen, S.-r.; Huang, Q.-y.; Chen, W.-c.; Xia, T.; Shi, Y.-c.; Gao, H.-z.; Shi, Q.-y.; Lin, S. Repair abilities of mouse autologous adipose-derived stem cells and ShakeGel^{TM}3D complex local injection with intrauterine adhesion by BMP7-Smad5 signaling pathway activation. *Stem Cell Res. Ther.* **2021**, *12*, 191.

https://doi.org/10.1021/acsomega.1c02117
ACS Omega 2021, 6, 23067−23075